Photoactive Pb^{3+} host lattice ions in photorefractive $Pb_5Ge_3O_{11}$ investigated by magnetic resonance techniques

2001 J. Phys.: Condens. Matter 13 3767

(http://iopscience.iop.org/0953-8984/13/16/307)

INSTITUTE OF PHYSICS PUBLISHING JOURNAL OF PHYSICS: CONDENSED MATTER

J. Phys.: Condens. Matter **13** (2001) 3767–3778 www.iop.org/Journals/cm PII: S0953-8984(01)20983-7

Photoactive Pb^{3+} host lattice ions in photorefractive $Pb_5Ge_3O_{11}$ investigated by magnetic resonance techniques

H J Reyher, M Pape and N Hausfeld

FB Physik, Universität Osnabrück, D-49069 Osnabrück, Germany[1]

E-mail: hjreyher@physik.uni-osnabrueck.de

Received 16 January 2001, in final form 26 March 2001

Abstract

In photorefractive $Pb_5Ge_3O_{11}$ and $(Pb_{0.98}Ba_{0.02})_5Ge_3O_{11}$ crystals, Pb^{2+} host lattice ions can be recharged by visible light to Pb^{3+}. The magnetic and structural properties of this hole-trapping centre, metastable at low temperatures, are characterized by means of electron paramagnetic resonance. The axial g-parameters are found to be $g_\perp = 2.0005(4)$ and $g_\parallel = g_\perp + 0.0064(3)$ and the ^{207}Pb hyperfine interaction constants are $A_\perp = 34.77(5)$ and $A_\parallel = 34.64(5)$ GHz. This information is correlated with optical properties derived from optically detected magnetic resonance via the magnetic circular dichroism of the absorption. In this way, broad photochromic absorption bands extending from the band edge to 1.9 eV can be attributed to the Pb^{3+} centre. Several observations give evidence that the Pb^{3+} centre is involved in the holographic recharging effects observed in lead germanate.

1. Introduction

Lead germanate, $Pb_5Ge_3O_{11}$, is an interesting material. Its ferroelectricity was first described by Iwasaki *et al* [1] and Nanamatsu *et al* [2]. Since then, a great number of publications have dealt with its dielectric and electro-optic properties (for a more recent publication, see reference [3]). However, only few investigations considered the photorefractive properties of this crystal [4–6]. Holographic gratings with slow and fast build-up times were found and the photorefractive sensitivity for the slow grating is comparable to that of $LiNbO_3$ [5]. In view of this and the rather favourable crystal growth properties of lead germanate, it is astonishing that, except the work of Yue *et al* [5, 6], no attempt has been made to improve the photorefractive properties of this material by doping with foreign ions. As is well known, such dopants often influence the electro-optic and charge-transport properties drastically. It turned out [5, 6], however, that the introduction of ions such as Fe or Rh led to a decrease of

[1] Fax: +49-541-9692670.

0953-8984/01/163767+12$30.00

the diffraction efficiency. It has therefore been proposed that intrinsic defects act as charge traps in the photorefractive process [5].

The present work will show that diamagnetic Pb^{2+} ions on specific regular Pb sites can be recharged metastably at low temperatures to paramagnetic Pb^{3+} by optical illumination. These Pb^{3+} centres are good candidates for being the just-mentioned intrinsic 'defects' which are involved in the holographic process, at least for the fast gratings.

In addition, the EPR of Pb^{3+} centres is interesting in itself, since it enriches the EPR data for ions with the s^1 configuration (for Pb^{3+}, see [7–15]). The spectra of Pb^{3+} exhibit the characteristic hyperfine pattern for the odd lead isotope ^{207}Pb and the interpretation of this hyperfine interaction and the g-values yields interesting information on the orbitals of the unpaired spin. This will be discussed below.

2. Experimental procedure

A nominally undoped crystal and a $(Pb_{0.98}Ba_{0.02})_5Ge_3O_{11}$ solid-solution sample were investigated extensively. For an oxidized pure sample and a Ni-doped crystal, only the effect of photo-generation of Pb^{3+} was verified. The crystals were grown at the Crystal Growth Laboratory of Dr H Hesse at the Physics Department in Osnabrück. The Czochralski technique was used; details are described elsewhere [5]. X-ray-oriented specimens were cut and polished. Subsequently, these samples were poled by applying an electric field (0.3 kV cm^{-1}) when cooling down to room temperature and thus passing through the paraelectric-to-ferroelectric phase transition. The single-domain state was checked by piezoelectric and pyroelectric measurements.

A pure and a Ba-containing crystal were chosen for magnetic resonance experiments, since these two specimens showed the highest and the lowest refractive index modulation Δn, respectively, in holographic experiments [5]. The observed Δn is directly related to the effective density N_{eff} of the photoactive centre (reference [16] and see below). Therefore, if this photoactive centre is an intrinsic defect, the density of this defect (in its minority charge state) should be different for these two samples. This will be verified below. The existence of the main mechanism of Pb^{3+} photo-generation in all samples investigated, including the Ni-doped and the oxidized pure crystal, indicates that Pb^{3+} is an omnipresent charge-trapping centre in $Pb_5Ge_3O_{11}$.

The EPR spectra were recorded with a CW X-band spectrometer. A silica rod serving as sample holder allowed the illumination of the crystal during the measurement and, hence, the *in situ* study of recharging processes. Measurements of the magnetic circular dichroism (MCD), optically detected magnetic resonance (ODMR) and photochromism were performed with a standard set-up as described, e.g., in reference [17] using an optical magnet–cryostat. For recharging experiments an argon-ion laser or a xenon arc lamp was used. The spectral sensitivity of the recharging effect was not investigated.

3. Experimental results

3.1. Conventional EPR

The results presented below were obtained for both extensively investigated samples. After cooling the crystals in the dark to temperatures well below liquid nitrogen temperature for EPR measurements, the known Cu^{2+} spectrum [18] is observed. This is shown as curve (a) in figure 1 for the orientation $\vec{B} \parallel \vec{c}$, where $\vec{c}$ is the threefold crystal axis. The attribution of the lines to the (predominant) spectrum (a) [18] of Cu^{2+} is confirmed by an excellent fit of the

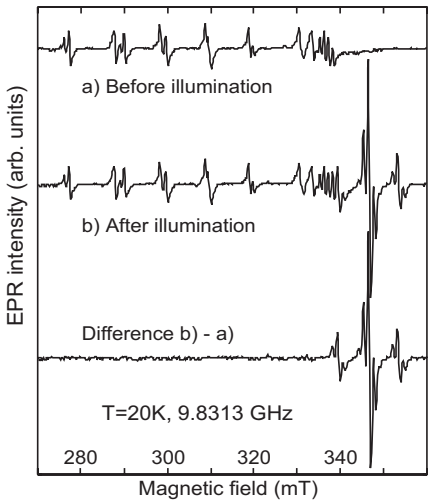

Figure 1. The X-band EPR spectrum of as-grown $Pb_5Ge_3O_{11}$ at $T = 75$ K, 9.26 GHz. The lowest trace corresponds to the difference between the spectrum after (b) and before (a) illumination with unfiltered light from a Xe lamp.

calculated resonance positions to the measured values using the known parameters [18] of the spin Hamiltonian. The EPR spectrum (b) was recorded under the same conditions as before, but after approximately 30 seconds of illumination at the same temperature with unfiltered light from a 100 W Xe lamp, guided to the probe by fibre-optics and the crystal holder. New signals show up which we shall assign below to Pb^{3+} ions. The third spectrum in figure 1 is obtained simply by subtracting the first from the second one. The result shows that the Cu signal intensities remain unchanged under the given illumination conditions.

In addition to the Cu EPR signal just mentioned, an unidentified signal from an axial centre with $g_{\parallel}^{\text{eff}} \approx 2.01$ and $g_{\perp}^{\text{eff}} \approx 6$ was observed. As in the case of Cu^{2+}, this centre was not affected by illumination. It is therefore unlikely that these two centres are involved in the holographic process.

3.2. EPR properties of Pb^{3+}

The EPR signals after illumination displayed in figure 1 are easily identified as being due to Pb^{3+} because of the characteristic hyperfine interaction, visible for the odd isotope ^{207}Pb with nuclear spin $\frac{1}{2}$ (22.1% abundance). The signals corresponding to transitions of $^{207}Pb^{3+}$ are found at ≈550 mT and ≈1100 mT for X-band frequencies (9.5 GHz). In table 1 the values of the axial hyperfine tensor **A** are given as well as the data for Pb^{3+} centres in some other oxide hosts for comparison. The similarity with the parameter values for Pb^{3+} in $CaWO_4$, CaO and $Pb(Zr_{1-x}Ti_x)O_3$ is striking.

Taking into account the different transition probabilities for the $I = 0$ and the $I = \frac{1}{2}$ lines, the relative intensities of the corresponding signals were found to be consistent with the natural abundance of the various Pb isotopes. The parameters given in the table were obtained by a fit to the angular dependence of the resonance fields for a 180° rotation of the magnetic field $\vec{B}$ in a plane containing the threefold axis $\vec{c}$. A variation of the orientation of $\vec{B}$ perpendicular to $\vec{c}$ resulted in no shift of the Pb lines within the experimental error of ≈0.1 mT. This establishes the axial character of the centre and means that the Pb^{3+} ion is on a site with C_3 symmetry—that

Table 1. EPR parameters of Pb^{3+} in $Pb_5Ge_3O_{11}$ and other oxides.

Host	$g_\parallel$	$g_\perp$	$A_\parallel$ (GHz)	$A_\perp$ (GHz)	Reference, remark
$Pb_5Ge_3O_{11}$	$g_\perp + 0.0064(3)$	2.0005(4)	34.64(5)	34.77(5)	C_3 site; equal g-values for odd and even isotopes
$CaWO_4$	1.9919	1.9889	38.410	38.437	[12], D_{2d} site
CaO	1.999		35.7		[11], cubic site
ZnO	2.013		26.95		[11], cubic site
$Pb(Zr_{1-x}Ti_x)O_3$	1.995		36.03		[15], ceramics

is, most probably on a regular Pb site. This finding is further confirmed by the resolved part of the superhyperfine structure, to be discussed now.

As one may see in figure 1, superhyperfine (SHF) interaction with distant ^{207}Pb nuclei leads to a partially resolved structure of the $I = 0$ resonance line. The same is observed for the $I = \frac{1}{2}$ lines at 550 and 1100 mT (for 9.5 GHz). There are two strong side bands separated by $\approx$7 mT from the central line and weaker ones at about double the distance (not visible in figure 1). These satellites are shown in the following to be due to two nearest-neighbour ^{207}Pb nuclei. A finer structure ($\approx$2.6 mT) arising from more distant ^{207}Pb nuclei is not resolved and has not been analysed. A rotation of $\vec{B}$ in the plane perpendicular to the $\vec{c}$-axis shows again no variation of both the 7 mT and the 14 mT satellites. This means that the interacting distant nuclear spins are also located on the $\vec{c}$-axis leading to axial SHF tensors $\mathbf{A}^{\mathbf{a},\mathbf{b}}$. The angular dependence of the satellite positions for a rotation in a plane containing $\vec{c}$ is shown in figure 2. The fit shown was obtained by assuming two magnetically inequivalent nearest neighbours (NN) **a** and **b** with $A^{\mathbf{a}}_\parallel = 155.4$, $A^{\mathbf{a}}_\perp = 130.9$, $A^{\mathbf{b}}_\parallel = 130.2$, $A^{\mathbf{b}}_\perp = 130.4 \times 10^{-4}$ cm^{-1}. These values have been found by fits to the branches labelled **a** and **b**, which result for the case where only one NN is ^{207}Pb. The lines for the case of both NN being odd isotopes (**a** + **b**) are not fitted but are obtained with the A-values found for branches **a** and **b**. The good agreement with the experimental points for **a** + **b** validates these A-values. We also checked by signal integration that the relative intensities of the SHF signals **a**, **b** and **a** + **b** agree with the relative probabilities for these different cases according to the isotopic abundances. All of these findings lead to the conclusion that Pb^{2+} ions from *only one* of the six mutually different C_3 sites of Pb in $Pb_5Ge_3O_{11}$ [19] can be photo-recharged to Pb^{3+} metastably. Otherwise a more complicated SHF pattern would be obtained. This surprising finding will commented on in section 4. The specific Pb site will be labelled x. One of the six possible C_3 sites, which are rather similar to each other, is shown in figure 3. Pb5 has been chosen arbitrarily to represent the ion at position x. Nearest neighbours **a** and **b** then correspond to positions Pb3A and Pb3B (labels according to reference [19]). We shall now argue that the recharging process actually represents the trapping of a hole at such a Pb_x ion after electron–hole generation by band–band transitions.

The fact that the Pb^{3+}_x centre has to be interpreted as a trapped *hole* follows from the substantially reduced hyperfine interaction as compared to the free-ion case. The isotropic part of **A**, $a = \frac{1}{3}(2A_\perp + A_\parallel)$, amounts to only 45% of that of the free Pb^{3+} ion (77.9 GHz [20]). Hence the density probability of the unpaired spin at the nucleus is reduced by this amount. This reduction is commonly interpreted as being due to ligand covalency and is expressed by setting up symmetry-adapted molecular orbitals for the cluster consisting of the metal ion and the ligands, which are six oxygen ions in our case, as shown in figure 3. In this *ansatz*, the orbital part of the unpaired spin Φ is not simply the 6s wavefunction of the free ion but contains symmetry-allowed linear combinations χ of oxygen 2p functions [21], i.e., $\Phi = c_s$ Pb 6s+$c_\chi \chi$, the cs being appropriate coefficients. Thus the spin density at the ^{207}Pb nucleus and, hence,

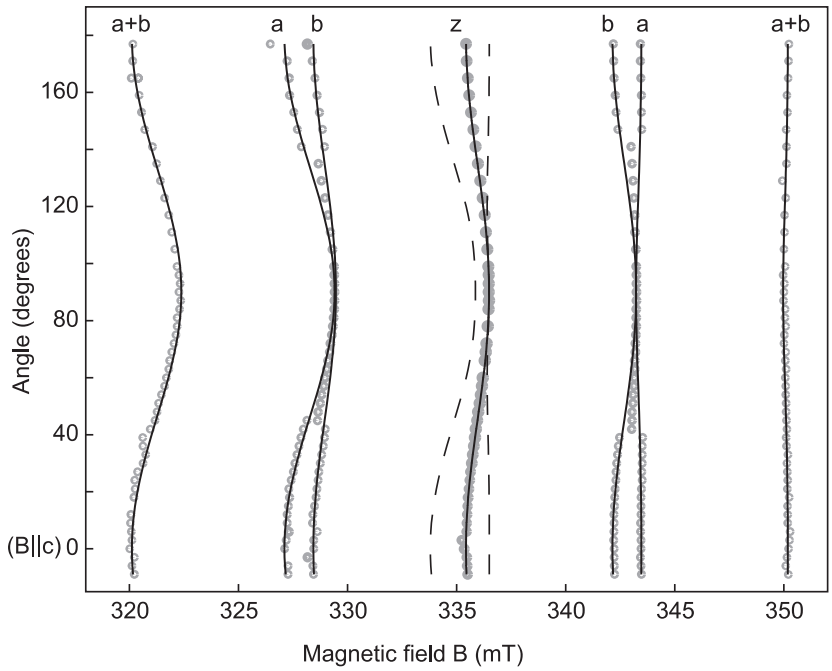

Figure 2. As-grown $Pb_5Ge_3O_{11}$. The angular dependence of the superhyperfine structure of the EPR line arising from even isotopes ($I = 0$) for rotation of the magnetic field in a plane containing the $\vec{c}$-axis. Dots represent experimental points; lines are fit results. Branch z arises from centres with no ^{207}Pb nearest neighbour (NN); **a** and **b** refer to lines arising from centres with only one (nearly equivalent) ^{207}Pb NN. **a** + **b** represent weak resonances arising from those centres where both NNs **a** and **b** are ^{207}Pb. In figure 3 these neighbours are labelled Pb3A and Pb3B. The dashed lines near z correspond to the case of **a** + **b**, but with opposite nuclear spins. Corresponding experimental signals cannot be resolved on the large central line z. $T = 50$ K, 9.56 GHz.

a are diminished. Also the admixture of the excited 6p orbitals of lead with the ground state leads to the same effects. An admixture of $6p_z$ is allowed by symmetry (no inversion centre) and it might be significant here since band formation may 'pull down' the energy of 6p states[1]. Admixture of 6p has been proposed by Warren *et al* [15] to explain the EPR linewidth of $^{207}Pb^{3+}$ transitions in lead zirconate titanate ceramics caused by an anisotropic tensor **A**. However, we may conclude from the negative sign of the anisotropic part of **A**, $b = \frac{1}{3}(A_\parallel - A_\perp) = -43(2)$ MHz (observable here, in a single crystal, in contrast to the case for ceramics [15]), that the $6p_z$ contribution to the ground state is negligible, since p_z admixture leads to positive b [23]. Alternatively, one has to assume that instead the covalent part χ of Φ is responsible for the observed negative sign of b. This has been assumed quite similarly for the case of $CaWO_4$:Pb^{3+}, where also $A_\parallel < A_\perp$ is found [12], in tetragonal symmetry. A model calculation concerning this point would be very informative. Such a calculation is also necessary to interpret the g-values of Pb_x^{3+} in $Pb_5Ge_3O_{11}$. At this stage, one may just state that the values of **g** and **A** fit well into the phenomenological correlation diagram shown in reference [11], where parameters for several Pb-doped compounds are compared. The subscript x is omitted from Pb^{3+} in the following for convenience.

[1] The lowest 6s6p level ($^3P_1$) of isoelectronic Hg atoms is at 4.88 eV above the ground state. In band-structure calculations, Robertson *et al* [22] find in lead zirconate titanate a contribution of Pb 6p to the bottom of the conduction band (band gap ≈3 eV).

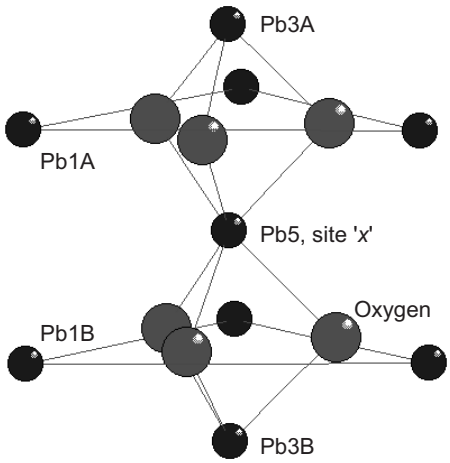

Figure 3. A fragment of the $Pb_5Ge_3O_{11}$ lattice with a site-*x* candidate (Pb5) at the centre. After illumination, a hole is trapped at this ion, recharging it to paramagnetic Pb^{3+}. The nearest oxygen ions are shown as well as the nearest-neighbour C_3 lead ions (Pb3A, Pb3B) and the next-nearest Pb ions (Pb1A, Pb1B), which are on C_1 sites. Triangles connecting the latter species reflect the threefold symmetry. The Pb ions are labelled according to [19].

3.3. Pb^{3+} concentration

For comparison with results from holographic experiments [5] it is essential to obtain a quantitative estimate of the Pb^{3+} concentration, which can be reached in equilibrium by illumination at low temperatures. To this end, a Si:P sample with known phosphorus content has been inserted in the EPR cavity together with the $Pb_5Ge_3O_{11}$ specimens. This Si probe showed only relatively weak signals from P clusters between the two hyperfine signals from isolated phosphorus [24], so we may assume the phosphorus atoms to be essentially isolated. The P^0 as well as the Pb^{3+} signals of the even isotopes, arising upon illumination at approximately the same magnetic field, have been measured at 15 K under identical conditions as functions of microwave power. This is essential since at these low temperatures, necessary for the P^0 detection, the Pb^{3+} signals saturate easily. The illumination was applied until the EPR signal intensity of Pb^{3+} did not increase further. The saturation of the photogeneration did not depend on the light intensity used. By integrating the EPR lines we arrive at $[Pb^{3+}]^{pure} = 5(2) \times 10^{16}\ cm^{-3}$ for the undoped crystal and $[Pb^{3+}]^{Ba} = 3.7(2.0) \times 10^{16}\ cm^{-3}$ for the crystal containing barium. These figures will be related to effective charge densities measured by holographic methods in the last section.

It is also interesting to note the densities of the unintentionally introduced copper ions. Since the Cu^{2+} spectrum consists of a great number of lines, it is difficult to integrate properly and we can only quote as crude estimates the concentrations $[Cu^{2+}]^{pure/Ba} = 1.5/2 \times 10^{16}\ cm^{-3}$. The somewhat higher value for the Ba crystal supports the assumption, already mentioned above, that Cu ions are unimportant for the holographic recharging processes, because this crystal showed no slow grating and lesser efficiency for the fast grating as compared with the pure one [5].

3.4. Photochromism, MCD and ODMR

The generation of Pb^{3+} by illumination induces a paramagnetic MCD, which will be attributed to this ion by the tagged-MCD method (see below). Simultaneously, an increase of optical

absorption (photochromism) arises. The corresponding photochromic spectrum $\Delta\alpha$ and the spectral dependence of the photo-generated MCD are both shown in figure 4. Below $\approx$3 eV the transmitted intensity of the probe light becomes too weak for MCD and absorption measurement.

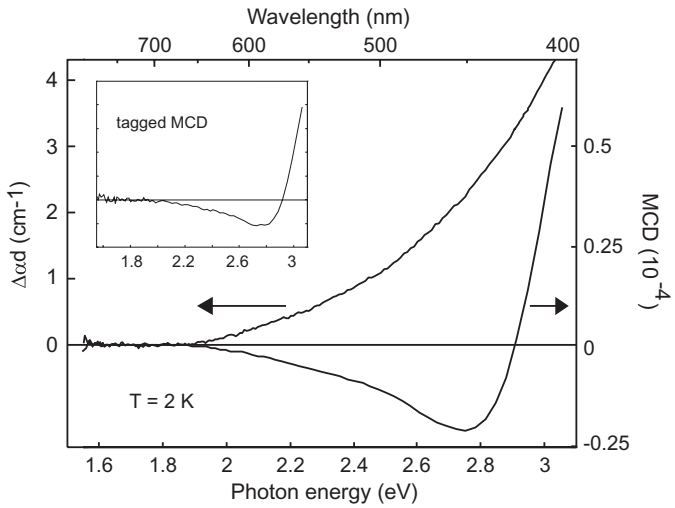

Figure 4. Photoinduced MCD and the absorption coefficient $\Delta\alpha$ of Pb^{3+} in $Pb_5Ge_3O_{11}$. The MCD spectrum is found after sample illumination only and is stable at 2 K for more than six hours at least. The same applies to the photochromism $\Delta\alpha$. Before illumination the measured MCD signal represents the zero line on the given scale. The right-hand ordinate is in relative units as explained in [17].

The interrelation between absorption and paramagnetic MCD spectra is based on the fact that they are composed from bands of the same shape, if these bands are not too sharp [25]. If the spectra consist of two (or more) overlapping subbands, one often encounters a situation where these subbands have opposite MCD signs and are thereby resolved, whereas they are not resolved in absorption. In other words, the MCD structure observed is typical for the $\Delta\alpha$ spectrum. A quantitative description of the MCD structure of Pb^{3+} would require information on the excited states of this ion in $Pb_5Ge_3O_{11}$. Above, we suggested, by reference to the case of lead zirconate titanate, that the energy of 6p states may be lowered by band formation, falling to the bottom of the conduction band of $Pb_5Ge_3O_{11}$. The photochromic absorption might thus correspond to an electric dipole-allowed transition to 6p orbitals. This would explain the strength of the induced absorption and the existence of the (at least) two observed MCD bands with opposite sign[2]. Also, quite similar spectra have been found for the 6s ion Bi^{4+} in sillenites [27]. In view of this and because of the striking similarity of the low-energy wings of the two spectra, we assume that the photochromism $\Delta\alpha$ is due to Pb^{3+} alone.

We could not find evidence for the existence of other centres being recharged in the spectral region depicted in figure 4. Therefore we shall use the photoinduced $\Delta\alpha$ in this region

[2] In a single-electron picture, the Pb^{3+} absorption would be described as a 6s–6p transition. It has been shown for the As_{Ga} antisite in GaAs (single hole) that, in axial symmetry, the MCD from an s–p transition consists of three bands, two of which have opposite sign [26]. Applying a single-electron picture does not contradict the single-hole picture useful for the ground state. Both are simplifications of adequate multi-electron states containing configurations, e.g., $6s2p^n$ (a hole in a 6s orbital) or $6s^22p^{n-1}$ (a hole in an oxygen 2p orbital), making up the ground state. Possible singly excited configurations are $6p2p^n$ and $6s6p2p^{n-1}$. The transition between these configurations corresponds to an electron 6s–6p transition of Pb.

to monitor the thermal decay of the Pb^{3+} centre. But before doing so, we want to make clear that the MCD is fully related to Pb^{3+} by using ODMR and the tagged-MCD method.

Figure 5 shows the ODMR signals at 70 GHz when monitored by the MCD at 450 nm. With 35 GHz, the same situation is found. The positions of all signals agree, within error, with the values calculated using the parameters from the EPR. Also the SHF structure is the same as that seen by means of EPR. It can be resolved for all lines only by making very slow field scans (see the inset in figure 5 for an example), since the longitudinal relaxation time T_1 is of the order of a minute at low temperatures. The agreement between the EPR and ODMR ensures that the same Pb^{3+} centres are observed in the two cases. This, in turn, allows the attribution of the observed MCD spectrum to Pb^{3+} by the tagged-MCD method [17]. In this technique, the height of a certain ODMR dip is recorded as a function of photon energy, yielding the paramagnetic contribution of the resonant centre to the total MCD. In the present case, the tagged-MCD and MCD methods show the same spectral dependence within experimental error. This means simply that the photoinduced MCD has to be fully attributed to the Pb^{3+} centre.

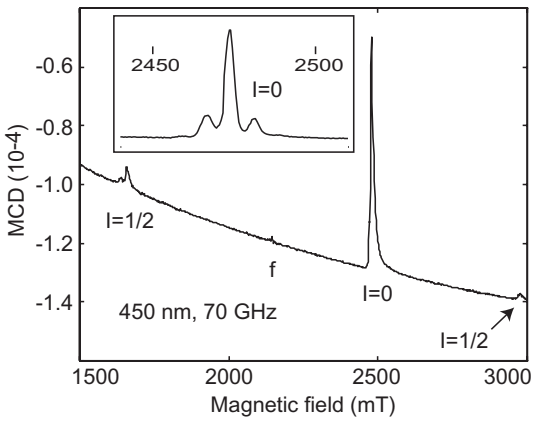

Figure 5. MCD of Pb^{3+} in $Pb_5Ge_3O_{11}$ at 450 nm as a function of the magnetic field B. The various dips are the ODMR signals for even isotopes ($I = 0$) and for ^{207}Pb ($I = 1/2$). The so-called forbidden transition of the $I = 1/2$ system is labelled 'f'. The superhyperfine structure is only visible at very slow scan rates (see the inset) because of the very long T_1-time of Pb^{3+} at 2 K (of the order of minutes).

In summary, the EPR 'fingerprint' has been transferred to the photochromic spectrum $\Delta\alpha$, as we had already correlated the MCD with $\Delta\alpha$.

3.5. Thermal decay of Pb^{3+}

The photoinduced absorption $\Delta\alpha$ is now used as a monitor for the Pb^{3+} concentration and the thermal decay of this metastable centre is studied. The samples were illuminated at a certain temperature T with white light from a Xe arc lamp until saturation of the Pb^{3+} concentration was achieved. Then, keeping T constant, the recovery of the optical transmission at 420 nm was measured using a weak probe beam. The resulting decay curves of $\Delta\alpha$ could be fitted satisfactorily by a single exponential $\propto e^{-t/\tau}$. Figure 6 shows $\ln(\tau)$ as function of $1/T$, i.e., Arrhenius plots, for the data obtained in this way.

A substantial error for the activation energy may result from the large scatter of the data points from the photochromic experiments, especially for the Ba-containing crystal. Nevertheless it is clear from figure 6 that the extrapolated time constants τ of the Pb^{3+} decay

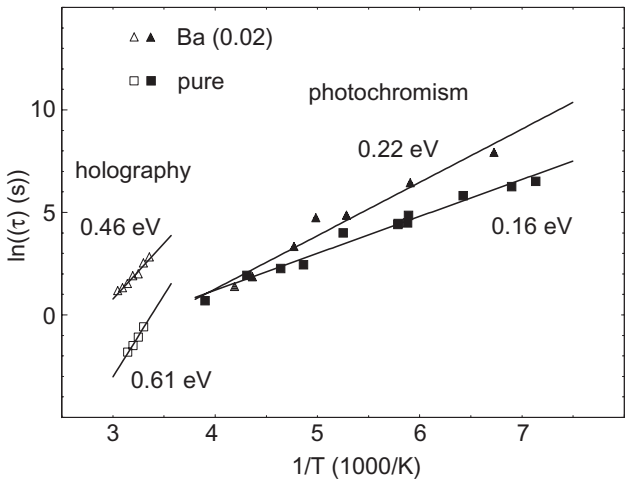

Figure 6. Arrhenius plots for the thermal decay constants of photo-generated Pb^{3+} ions. Corresponding plots for the decay of the fast holographic gratings [5, 6] are added. The activation energies found from the different observations are indicated.

at room temperature are shorter than or comparable to those obtained for the decay of the fast holographic gratings [5] and that the activation energies are lower at least by a factor of two. These findings will be discussed in the next section.

4. Discussion

We observe that Pb_x^{3+} centres are generated by illumination of the crystals. The simplest conceivable model for this process is shown in figure 7.

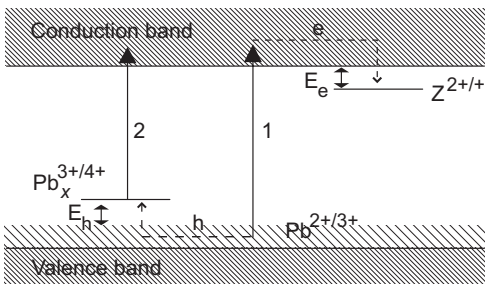

Figure 7. The model level scheme used to explain the observed recharging effects. See the text.

Localized recharging states (3+/4+) of Pb ions on sites x are assumed to be somewhat above the valence band, since localized holes, trapped at these sites, are observed by means of EPR at low T. The closeness to the valence band is justified in view of the observed (see section 3.2) delocalization of these holes onto oxygen orbitals. Consequently, Pb 6s and O 2p levels must be energetically close. Pb 6s character of the valence band is supported by the Robertson *et al* band-structure calculations on lead zirconate titanate [22]. Transitions ('1' in figure 7) from shallow valence-band-like levels (indicated by wide hatching) to the conduction band are considered to be a primary process for the photoionization to Pb_x^{3+}. These shallow

levels are invoked because they may account for the hump in absorption below the band edge, which is observed in pure as well as in many doped $Pb_5Ge_3O_{11}$ crystals [5, 6]. In addition, transitions from these levels can also explain why recharging and hologram writing with green (514 nm) laser light, definitely below the band edge, is feasible. The holes are trapped at a Pb_x ion at low T populating the (3+/4+) recharging level. At elevated temperatures they may stay mobile and may account for the electron–hole competition observed in holographic experiments. The photoelectrons are captured at unknown centres Z. Optical transitions ('2' in figure 7) from the $Pb_x^{3+/4+}$ level to conduction-band-like states account for photochromism and MCD.

It is surprising that the symmetry of the trapped holes, i.e. of Pb_x^{3+}, is C_3, the highest site symmetry in $Pb_5Ge_3O_{11}$. Usually, holes localize at symmetry-lowering defects like the Mg vacancy forming the famous V^- centre in MgO [28], for example. In view of the structure of lead germanate, it is difficult to conceive of a defect adjacent to Pb_x^{3+} which conserves both symmetry and the approximate equivalence of the nearest Pb neighbours on the C_3 axis, as found in the superhyperfine structure. The latter finding rules out symmetry-conserving adjacent interstitials on the C_3 axis from being trapping centres. These considerations apply in particular to the Z centre, and one has instead to assume a larger separation of several inter-ionic distances for this electron trap. Consequently, we have to invoke a self-trapping mechanism for the hole at Pb_x. This raises the question of why only one of the six mutually different C_3 sites is favoured. All of these six sites are structurally very similar and there are no simple arguments as regards how to assign the energetically most favourable one. Without the help of quantum chemical calculations, such an assignment would be too speculative.

Only a small fraction ($\approx 5 \times 10^{-4}$) of the Pb_x^{2+} sites available are recharged at low T. This is most easily interpreted in terms of a limited number of electron traps Z, which accommodate the photoelectrons of the ionized Pb_x^{2+} ions. Unfortunately, we could not identify these rechargeable centres Z, neither using EPR nor using photochromism. One of the two charge states, Z^+ or Z^{2+}, must clearly represent a paramagnetic centre. As usual, one has to assume that Z is not detectable by means of EPR because its resonance line is 'broadened beyond detection' by either homogeneous or inhomogeneous effects.

The participation of the Pb_x^{3+} centre in the holographic processes will be discussed now. We find that the Pb_x^{3+} centre, generated by homogeneous illumination, is unstable at room temperature, with recombination times of less than a second. If Pb_x^{3+} were to be one of the charge-trapping centres responsible for the slow, stable grating observed in reference [5], it would be difficult to conceive of a mechanism of stabilization of Pb_x^{3+} by the slow holographic process. In addition, the slow grating was only observed in pure $Pb_5Ge_3O_{11}$, whereas Pb_x^{3+} was found at similar concentrations in the Ba-containing crystal, and in a Ni-doped specimen, as well. Hence, the observations presented do not allow the microscopic characterization of the slow grating in pure $Pb_5Ge_3O_{11}$. However, we are now giving arguments as regards why the Pb_x^{3+} centre should be involved in the fast-grating formation [5].

First, Pb_x^{3+} is an intrinsic centre and can be generated by visible light illumination. These are prerequisites to obtaining agreement with the observation of similar holographic performance of crystals doped by a variety of impurity ions [5, 6]. Second, the density of this centre created by a certain illumination dose must be of the order of several 10^{16} cm^{-3}, since effective charge-trap densities, N_{eff}, of this order have been found in holographic experiments. The refractive index change Δn, observed there, is directly related to an effective density N_{eff} of charge traps, which is usually equal to either N^+ or N, whichever is the smaller density [16]. N^+ and N correspond to the densities of the photoactive centre in two adjacent charge states, which are available at the beginning of the build-up of the holographic grating, either in the dark or immediately after exposure to light. We identify $N = [Pb_x^{2+}]$ and $N^+ = [Pb_x^{3+}]$, where

the subscript 'x' indicates Pb ions on the specific C_3 site only, as found using EPR. Since there are $\approx 10^{21}$ cm^{-3} equivalent Pb^{2+} sites of type x, we must set N_{eff} equal to the number of Pb_x^{3+} ions generated at the beginning of the holographic recording. This number should be somewhat less than the $[Pb_x^{3+}]^{\mathrm{pure}} = 5 \times 10^{16}$ cm^{-3} and $[Pb_x^{3+}]^{\mathrm{Ba}} = 3.7 \times 10^{16}$ cm^{-3} found by means of EPR after exposure to saturating homogeneous illumination at low T. This is so, because the illumination for holography may not be saturating and it occurs at room temperature, where efficient recombination with Pb^{2+} occurs. Hence, the corresponding values $N_{\mathrm{eff}}^{\mathrm{pure}} = 1.16 \times 10^{16}$ cm^{-3} and $N_{\mathrm{eff}}^{\mathrm{Ba}} = 0.82 \times 10^{16}$ cm^{-3} from reference [5] fully agree with our attribution. This attribution is further supported by the observation that the ratio $N_{\mathrm{eff}}^{\mathrm{Ba}}/N_{\mathrm{eff}}^{\mathrm{pure}}$ is the same as $[Pb_x^{3+}]^{\mathrm{Ba}}/[Pb_x^{3+}]^{\mathrm{pure}}$ derived using EPR within experimental error.

The activation energies found for the hologram decay [5] are much higher than those obtained from the decay of $\Delta\alpha$, i.e., for the recombination of the electron trapped at Z and the hole at Pb_x^{3+}. This can be explained if one assumes that the average separation of the electron and hole traps, Z and Pb_x^{3+}, is rather small after homogeneous illumination. In this case no charge transport is required for recombination. Grating decay, on the other hand, requires charge transport to overcome the relatively large spatial separation of the charge carriers. Consequently, different effects are measured in the two cases, the activation energy for recombination of close defects on the one hand and the activation energy for long-range hopping between equal traps on the other. The spatial separation between Z and Pb_x^{3+} has been termed 'rather small' because the immediate neighbourhood is ruled out by the EPR data. As explained above, no symmetry lowering of the lattice site occupied by Pb_x^{3+} is observed.

5. Conclusions

We have identified lead host ions at specific sites x in $Pb_5Ge_3O_{11}$ which can be recharged optically to Pb^{3+}. This hole centre Pb_x^{3+} is metastable at low temperatures. We have provided evidence that Pb_x^{3+} is involved in the holographic process relating to the fast gratings. Only a small fraction of the Pb_x^{3+} centres available in the crystal can be recharged. This is ascribed to the limited number of electron traps needed for the metastable recharging process. So far, the photoelectron trapping centre Z has not been identifiable. The identification of this centre and suitable crystal treatment to increase its density would allow one to enhance the crucial holographic parameter N_{eff} for $Pb_5Ge_3O_{11}$ drastically. This would make lead germanate a most promising photorefractive substance.

Acknowledgments

We thank Professor O F Schirmer for active help and fruitful discussions. The support of the Deutsche Forschungsgemeinschaft, SFB 225/C4-C2, is gratefully acknowledged.

References

[1] Iwasaki H, Sugii K, Yamada T and Niizeki N 1971 *Appl. Phys. Lett.* **18** 444
[2] Nanamatsu S, Sugiyama H, Doi K and Kondo Y 1971 *J. Phys. Soc. Japan* **31** 616
[3] Nanda Goswami M L, Choudhary R N P and Mahapatra P K 1998 *J. Phys. Chem. Solids* **59** 1045
[4] Królikowski W, Cronin-Golomb M and Chen B S 1990 *Appl. Phys. Lett.* **57** 7
[5] Yue X, Mendricks S, Hu Y, Hesse H and Kip D 1998 *J. Appl. Phys.* **83** 3473
[6] Yue X, Mendricks S, Nikolajsen T, Hesse H, Kip D and Krätzig E 1999 *J. Opt. Soc. Am.* B **16** 389
[7] Räuber A and Schneider J 1966 *Phys. Status Solidi* **18** 125
[8] Suto K and Aoki M 1967 *J. Phys. Soc. Japan* **22** 1307
[9] Shoemaker D and Kolopus J I 1970 *Solid State Commun.* **8** 435

[10] Kolopus J I, Finch C B and Abraham M M 1970 *Phys. Rev.* B **2** 2040
[11] Born G, Hofstaetter A and Scharmann A 1971 *Z. Phys.* **248** 7
[12] Born G, Hofstaetter A, Scharmann A and Vitt B 1974 *Phys. Status Solidi* b **66** 305
[13] Friebele E J 1977 *Proc. 11th Int. Congr. on Glass (Prague)* vol 3 (Prague: CVTS-Dum Techniky) p 87
[14] Hosono H, Nishii J, Kawazoe H, Kanazawa T and Ametani K 1980 *J. Phys. Chem.* **84** 2316
[15] Warren W L, Tuttle B A, McWhorter P J, Rong F C and Poindexter E H 1993 *Appl. Phys. Lett.* **62** 482
[16] Valley G C and Lam J F 1988 *Photorefractive Materials and Their Applications I* ed P Günter and J-P Huignard (Berlin: Springer)
[17] Spaeth J-M, Niklas J R and Bartram R H 1992 *Structural Analysis of Point Defects in Solid* (Berlin: Springer) ch 9
[18] Vazhenin V A, Gorlov A D, Krotkiĭ A I, Potapov A P and Starichenko K M 1989 *Sov. Phys.–Solid State* **31** 825
[19] Kay M I, Newnham R E and Wolfe R W 1975 *Ferroelectrics* **9** 1
[20] Schawlow A L, Hume J N P and Crawford M F 1949 *Phys. Rev.* **76** 1876
[21] Iida T and Watanabe H 1968 *Phys. Lett.* **26** A 541
[22] Robertson J, Warren W L, Tuttle B A, Dimos D B and Smyth D M 1993 *Appl. Phys. Lett.* **63** 1519
Warren W L, Robertson J, Dimos D B, Tuttle B A and Smyth D M 1994 *Ferroelectrics* **153** 303
[23] Weil J A, Bolton J R and Wertz J E 1994 *Electron Paramagnetic Resonance* (New York: Wiley)
[24] Feher G 1959 *Phys. Rev.* **144** 1219
[25] Stephens P J 1976 *Adv. Chem. Phys.* **35** 197
[26] Kaufmann U and Windscheif B 1988 *Phys. Rev.* B **38** 10 060
[27] Reyher H-J, Hellwig U and Thiemann O 1993 *Phys. Rev.* B **47** 5638
[28] Henderson B and Wertz J E 1977 *Defects in the Alkaline Earth Oxides* (London: Taylor and Francis)